© Universiti Tun Hussein Onn Malaysia Publisher's Office

IJIE

Journal homepage: http://penerbit.uthm.edu.my/ojs/index.php/ijie
ISSN : 2229-838X e-ISSN : 2600-7916

The International Journal of Integrated Engineering

Application of Non-Model Dependent Hybrid Higher-Order Differential Feedback Controller on Crane System

Haliru Liman[1], Nura Musa Tahir[2]*, Sani Godwin[2], Ejike C. Anene[1], Yakubu Shehu[2], Ahmad Bala Alhassan[3]

[1]Department of Electrical and Electronics Engineering,
Abubakar Tafawa Balewa University (ATBU) Bauchi, P.M.B 0248, NIGERIA

[2]Department of Mechatronics and System Engineering,
Abubakar Tafawa Balewa University (ATBU) Bauchi, P.M.B 0248, NIGERIA

[3]School of Mechanical Engineering, Xi'an Jiaotong University, Xi'an 710049, CHINA

*Corresponding Author

DOI: https://doi.org/10.30880/ijie.2020.12.04.012
Received 15 January 2019; Accepted 25 July 2019; Available online 30 April 2020

Abstract: Shipping of goods from one place to another in industries is commonly achieved with crane system. But such movement of the system results in undesirable sway which degrades the accuracy and safety. In this paper, hybrid control schemes of the model-dependent and non-model dependent filters and controllers are proposed for precise trolley position control and sway suppression of the crane systems. Output based filter (OBF) was designed using the output of the system, so it does not depend on the model of the system while time delay filters (TDF) were designed using the model parameters (i.e. natural frequency and damping ratio), in which Zero Vibration (ZV) and zero vibration derivative (ZVD) were considered. These depend on the model of the system and these filters are for sway suppression of the payload. In addition, proportional integral derivative (PID) controller and higher order differential feedback controller (HODFC) were incorporated with each filter separately for precise trolley position control. Based on the analysis of the simulation results, it was observed that a precise tracking of the payload was achieved with percentage of the sway reduction of the hybrid controllers as follows; PID-ZV=76%, PID-ZVD=88%, PID-OBF=96% HODFC-ZV=77%, HODFC-ZVD=79% and HODFC-OBF=95%. The hybrid controllers shown precise tracking and higher sway reduction control. But HODFC-OBF is a model-free control schemes, thus more robust.

Keywords: Crane, output-based, time-delay, sway, model-free, higher-order

1. Introduction

The transportation of payloads from one point to another can be achieved by the use of a machine known as a crane system, as shown in Fig. 1. The application of this system can be found in transportation as well as construction industries. In order to increase the production rate of these industries, it has then become necessary for crane maneuvering to be carried out as fast as possible with a minimum payload sway [1], [2].

The undesirable motion of the crane, such as swinging, twisting and load bouncing can be yielded due to the maneuvering of the payload by hoisting. These undesirable movements have negative effects on the production rate, crane safety, crane operational efficiency and precision in the position of the payload [3]. For many years, research work in suspended load oscillation control, such as the two-dimensional crane, has increased the curiosity of researchers in that area.

*Corresponding author: ramanujkumar22@gmail.com

Fig. 1 - A typical 2D gantry crane system [4]

A number of researchers classified the flexible structures oscillation control into feedback and feed-forward control strategies. The crane system oscillation control is therefore divided into two categories via feedback and feed-forward control techniques. The feedback control technique can be employed in instances where high precision is needed in the position of the load as well as in the estimation of the system, which tends to minimize the influence of undesirable oscillation. On the other hand, the feed-forward control technique is used when there is a need to adjust the input command signal so as to get rid of the system oscillation [5]. The combination of feedback and feed-forward control schemes can lead to the achievement of better system performance with negligible vibration. Also, the use of feed-forward control can help in easing the design of feedback control system [6].

More so, an effort has been made by many researchers to suppress the effect of system vibration for the reliability, safety and efficiency of rotary crane systems. Several open and closed-loop control schemes, such as the proportional integral derivative (PID) control [7-9], optimal control [10], [11] and artificial intelligence (AI) [12], have been highlighted. The horizontal boom motion control of rotary crane has been proposed in [13] using open-loop control technique. In [14], the feed-forward input shaping and low pass filtering (LPF) performances were investigated. However, the study showed that for erroneous natural frequency, LPF is not as robust as input shaping. According to [3], the practical application of input shaping scheme has been used by a number of researchers in different flexible structures after initially proposed by Singer and Searing. As induced oscillation in a flexible robot manipulator was suppressed by the application of the command shaping technique [15], it was discovered that zero vibratory response can be attained using this method. In [5] however, the use of flexible beams clarified that analysis of the sensitivity of ZV, ZVD and ZVDD as shapers to natural frequency errors can be performed while [16-18], showed how input shaping can be used in crane systems of other forms. Even though the combination of feedback and open-loop control can yield an efficient control system [20], external disturbances are likely going to affect open-loop controllers [19].

The straight transfer transformation (STT) can be used as a method of controlling rotary crane systems [21]. In a condition where parameters are not well represented or models with some certain level of inaccuracies are used, the adaptive sliding mode control (SMC) and the partial feedback linearization (PFL) techniques can be applied when dealing with rotary crane sway reduction [22]. Despite the ease associated with the design and implementation of the partial feedback linearization technique, changes in parameters such as the cable diameter and length have a significant influence on the technique whereas the sliding mode controller has found application in other cranes due to its robustness [23-25]. According to [26], excessive energy is given off in the sliding mode control technique which of course result in system failure.

Open-loop control schemes are cheap and easy to implement since no sensors required. However, they are sensitive towards external disturbances which may result in payload oscillations. Although closed-loop techniques are less sensitive to disturbances and parameter variations, they are slow due to the input delay in the feedback loop, hence less efficient. Therefore, the trade-off between safety (fewer payload oscillations) and efficiency (fast performance) of the crane's operations is a challenging problem. In this paper, a comparative analysis of hybrid controllers was presented. Model dependent time delay filter and non-model dependent output based filter were incorporated with non-model dependent HODFC controller. Then, these filters were also combined with PID controllers so as to validate the performances of the hybrid HODFC for precise tracking of the desired position of the trolley as well as suppressing the oscillations of payload.

The paper is organized as follows: Section one is the introduction. Model description of the system is presented in section two, whereas Section three presents the proposed controller design. Section four discusses the simulation results and in Section six, the conclusion is made.

2. Model Dynamics

Crane system is a machine which is used to load and offload goods as well as transport them from one point to another. It is mostly used for heavy machine installations and finds application in a nuclear plant, warehouse, seaport and construction industries etc. In this work, a laboratory-scale 2D crane system was used and its schematic diagram is represented in Fig. 2 [27].

As shown, the length of the cable, the angle of sway, the horizontal position of a trolley, the mass of trolley and the payload mass are respectively represented by *l, θ, x, M* and *m*. The Lagrange formulation was used in the derivation of dynamical equations based on the assumptions that the masses of the trolley and payload are point masses that move in the two-dimensional, x-y plane and that the tension that may cause the cable elongate is negligible. Thus, the following set of nonlinear equations describes the dynamics of the gantry crane system [28], as shown in Eq. (1);

$$F_x = (M+m)\ddot{x} + ml\left(\ddot{\theta}\cos\theta - \dot{\theta}^2\sin\theta + 2ml\dot{\theta}\dot{\theta}\cos\theta + ml\ddot{\sin}\theta\right) \tag{1}$$

$$l\ddot{\theta} + 2l\dot{l}\dot{\theta} + \ddot{x}\cos\theta + g\sin\theta = 0 \tag{2}$$

In order to design controller, there is the need to linearize the nonlinear equations. The linearization is achieved using the assumption that θ is very small (i.e. $\theta \approx 0$, $\sin\theta \approx \theta$ and $\cos\theta \approx 1$). Therefore, the linearized equations are shown in Eq. (2);

$$F_x = (M+m)\ddot{x} + ml\ddot{\theta} \tag{3}$$

$$l\ddot{\theta} + \ddot{x} + g\theta = 0 \tag{4}$$

Thus, the linearized model of Eq. (3) and Eq. (4) can be written in a state-space form of Eq. (5) as shown in Eq. (6), where A is the system matrix, B is the input matrix, C is the output matrix with x and as the output parameters under consideration. Also, the constant parameters of the system are illustrated in Table 1.

$$\dot{x} = Ax + Bu \quad ; \quad y = Cx \tag{5}$$

$$\begin{bmatrix}\dot{x}\\ \ddot{x}\\ \dot{\theta}\\ \ddot{\theta}\end{bmatrix} = \begin{pmatrix}0 & 1 & 0 & 0\\ 0 & 0 & \frac{m}{M} & 0\\ 0 & 0 & 0 & 1\\ 0 & 0 & -\frac{(M+m)g}{Ml} & 0\end{pmatrix}\begin{bmatrix}x\\ \dot{x}\\ \theta\\ \dot{\theta}\end{bmatrix} + \begin{bmatrix}0\\ \frac{1}{M}\\ 0\\ -\frac{1}{Ml}\end{bmatrix}F_x \quad ; \quad \begin{bmatrix}x\\ \theta\end{bmatrix} = \begin{pmatrix}1 & 0 & 0 & 0\\ 0 & 0 & 1 & 0\end{pmatrix}\begin{bmatrix}x\\ \dot{x}\\ \theta\\ \dot{\theta}\end{bmatrix} \tag{6}$$

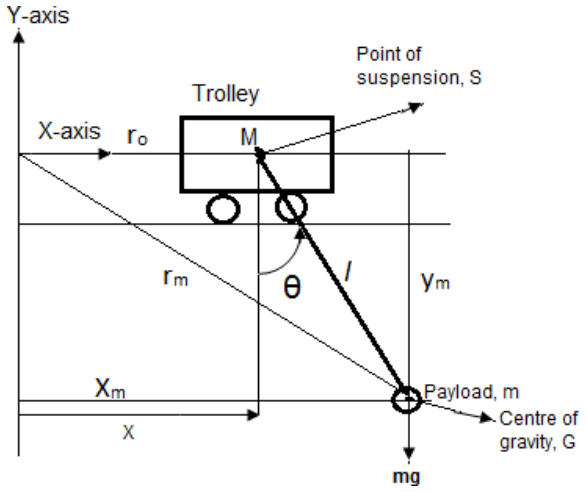

Fig. 2 - schematic diagram of the gantry crane system

Table 1 - System parameters

Parameter	Value /Unit
Mass of payload (m)	0.75 kg
Mass of trolley (M)	3 kg
Length of the cable (l)	0.75 m
Acceleration due to gravity (g)	9.81 ms^{-2}

3. Controllers Design

In this section, zero vibration (ZV) and zero vibration derivative (ZVD) filters and output-based filter (OBF), were designed and then incorporated with proportional integral derivative (PID) controller and higher order differential feedback controller (HODFC) separately for sway suppression and trolley position control of the crane system.

3.1 Time delay input shaping

The convolution process of a sequence of impulses with the reference input signal leads to the production of the time delay filters. Also, the damping ratios and natural frequency of the system were used to generate the time instants as well as the amplitudes of the impulse signals. Figure 3 shows the process of shaping the input signal. It consists of two impulses (ZV). Also, the system algorithm affirmation was achieved by considering a second-order response of a crane system as an under-damped system of the format in [29-32]. The open-loop transfer function of the system can be shown in Eq. (7), with natural frequency (ω) and damping ratio (ζ). Alternatively, Eq. (7) can be expressed in the time domain as shown in Eq. (8) [30];

$$G(s) = \frac{\omega^2}{s^2 + 2\zeta\omega s + \omega^2} \tag{7}$$

$$y(t) = \frac{A\omega}{\sqrt{\left(1-\zeta^2\right)}} e^{-\zeta\omega(t-t_0)} \sin\left(\omega(t-t_0)\sqrt{\left(1-\zeta^2\right)}\right) \tag{8}$$

Thus, with the amplitude and time instant of the impulse designated by A and t_0 respectively. However, applying superposition theorem on Eq. (8) leads to Eq. (9). Similarly, the amplitude of the residual vibration can be determined from trigonometric function as shown in Eq. (10);

$$y(t) = \sum_{i=1}^{n}\left[\frac{A_i\omega_n}{\sqrt{\left(1-\zeta^2\right)}} e^{-\zeta\omega_n(t-t_i)}\right] \sin\left(\omega(t-t_i)\sqrt{\left(1-\zeta^2\right)}\right) \tag{9}$$

$$\sum_{i=1}^{n} B_i \sin\left(\omega t + \beta_i\right) = A\sin(\omega t + \varphi) \tag{10}$$

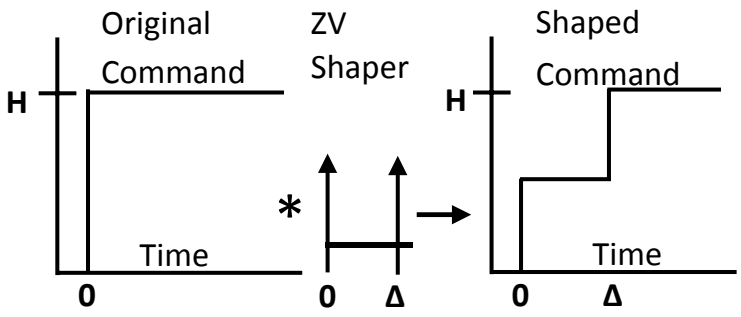

Fig. 3 - Process of shaping the input

Where

$$A = \sqrt{\left(\sum_{i=1}^{n} B_i \cos(\beta_i)\right)^2 + \left(\sum_{i=1}^{n} B_i \sin(\beta_i)\right)^2} \tag{11}$$

By equating terms in Equations (9) and (10), Equation (12) is obtained as;

$$B_i = \frac{A_i \omega_n}{\sqrt{\left(1-\zeta^2\right)}} e^{-\zeta\omega_n(t-t_i)} \tag{12}$$

The amplitude of residual oscillation can be obtained through the evaluation of Eq. (11) taken at the time of final impulse, $t = t_n$. By combining (11) and (12) and factorizing the constant part of the coefficients gives Equation (13);

$$A = \frac{\omega}{\sqrt{\left(1-\zeta^2\right)}} e^{-\zeta\omega t_n} \sqrt{R_1^{\,2} + R_2^{\,2}} \tag{13}$$

Where

$$R_1 = \sum_{i=1}^{n} A_i e^{\zeta\omega t_i} \sin\left(\omega t_i \sqrt{\left(1-\zeta^2\right)}\right) \tag{14}$$

$$R_2 = \sum_{i=1}^{n} A_i e^{\zeta\omega t_i} \cos\left(\omega t_i \sqrt{\left(1-\zeta^2\right)}\right) \tag{15}$$

The amplitude of the residual oscillation for unity magnitude at $t = 0$ can be determined using Eq. (16) while the percentage residual vibration can be determined from dividing Eq. (13) by Eq. (16) as shown in Eq. (17);

$$A_{\uparrow} = \frac{\omega}{\sqrt{\left(1-\zeta^2\right)}} \tag{16}$$

$$R = \frac{A}{A_{\uparrow}} = e^{-\zeta\omega(t_n)} \sqrt{R_1^2 + R_2^2} \tag{17}$$

To obtain ZV, the values of R_1 and R_2 are set to zero after the final impulse, which serves as the constraint of ZV while the summation of the amplitudes of the shaper to the impulse is taken as unity. The constraints of summation are obtained as shown in Eq. (18);

$$\sum_{i=1}^{n} A_i = 1 \tag{18}$$

The By setting the time instant of the first impulse to zero ($t_1 = 0$) and using ZV constraints leads to the ZV parameters as in Eq. (19);

$$\begin{bmatrix} A_i \\ t_i \end{bmatrix} = \begin{bmatrix} \frac{1}{1+k} & \frac{k}{1+k} \\ 0 & \tau_d \end{bmatrix} \tag{19}$$

Where

$$\tau_d = \frac{\pi}{\omega\sqrt{\left(1-\zeta^2\right)}} \tag{20}$$

$$k = e^{\frac{-\pi\zeta}{\sqrt{\left(1-\zeta^2\right)}}} \tag{21}$$

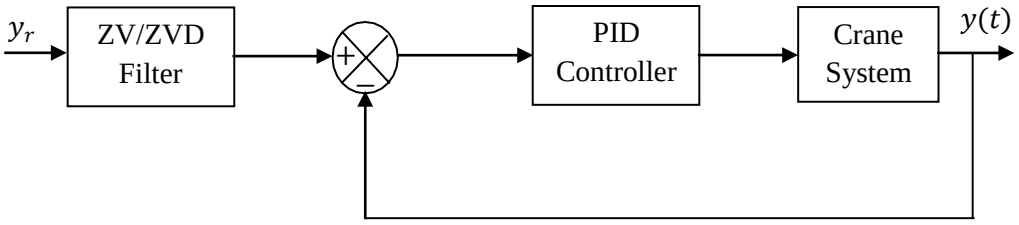

Fig. 4 - block diagram of PID-ZV/ZVD controllers

For the improvement in the frequency error robustness, the derivatives of R_1 and R_2 are taken as zero. This can be shown in Eq. (22);

$$\frac{\partial^i R}{\partial \omega^1}=0 \quad \text{and} \quad \frac{\partial^i R}{\partial \omega^2}=0 \tag{22}$$

However, the parameters of the three impulse ZVD shapers can be obtained by solving Equations (13), (16) and (18), which are the constraints equations. The result is shown in Eq. (23);

$$\begin{bmatrix} A_i \\ t_i \end{bmatrix}=\begin{bmatrix} \frac{1}{(1+k)^2} & \frac{2k}{(1+k)^2} & \frac{k^2}{(1+k)^2} \\ 0 & \tau_d & 2\tau_d \end{bmatrix} \tag{23}$$

Thus, the general representation of the ZV and ZVD shapers for implementation on the system with PID controller can be shown in the block diagram of Fig. 4, while the corresponding values of their parameters are shown in Table 2.

Table 2 – Parameters of shapers

Shaper	ZV	ZVD
A_1	0.5292	0.2801
A_2	0.4708	0.4983
A_3	-	0.2216
t_1 (sec)	0	0
t_2 (sec)	0.7889	0.7889
t_3 (sec)	-	1.5778

3.2 Out-Based Filter

To achieve the output-based input shaping filter (OBF) design of the plant, it is necessary to obtain the reference system design as shown in Eq. (24);

$$G_r(s)=\left[\frac{\omega_c}{(s+\omega_c)}\right]^n \tag{24}$$

Where the system bandwidth and system order are denoted by ω_c and n respectively and are dependent upon the response time of the system. Next is the decomposition of the output of the target system, y(t) as shown in Eq. (25) and Fig. 5, with the ith component of $y(t)$ and its coefficient represented by a_i and $y_i(t)$ respectively;

$$y(t)=\sum_{i=0}^{n} a_i y_i(t) \tag{25}$$

From Fig. 5, the target system is denoted by G(s) of Eq. (26), where $i = 0, 1, 2\ldots, n$ is the component of the target filter. The cost function in Eq. (27) was used in the minimization of the difference between responses of the target system $y(t)$ and that of the unit step of the reference system $y_r(t)$.

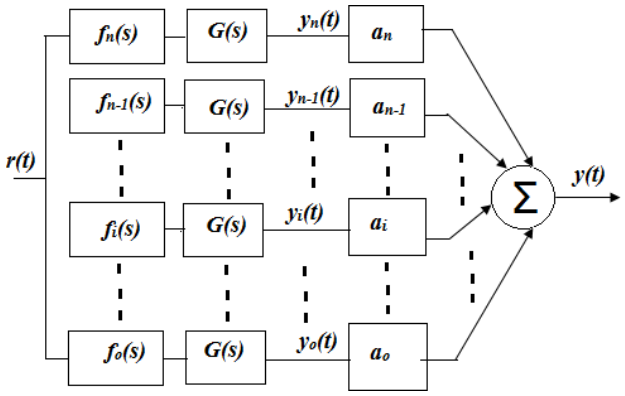

Fig. 5 - system decomposition using the input shaping filter

$$f_i(s) = \frac{s^i}{F_d(s)} \tag{26}$$

$$E = \int_0^T \omega(t)(y(t) - y_r(t))^2 dt \tag{27}$$

By the combination of Eq. (25) and (27), Eq. (28) is obtained as;

$$E(a_1, a_2, \ldots a_n) = \int_0^T \omega(t)((\sum_{i=0}^{n} a_i y_i(t)) - y_r(t))^2 dt \tag{28}$$

With $a_0 = \square_c^n$ and $a_1, a_2, \ldots, a_n$ as gains of the filter. Now by the selection of $a_0 = 3.5^4$, the vibration of the system tends to zero and the reference system is given in Eq. (29);

$$G_r(s) = \frac{150.0625}{s^4 + 14s^3 + 73.5s^2 + 171.5s + 150.0625} \tag{29}$$

With the relation in Eq. (30) was used to compute the gains of the filter in MATLAB as $a_2 = 564.1179$ and $a_4 = 34.6360$. Thus, the final filter to the system is expressed in Eq. (31). Finally, the general block diagram of the OBF for implementation on the system with PID controller can be shown in Fig. 6.

$$\begin{bmatrix} a_2 \\ a_4 \end{bmatrix} = \begin{pmatrix} s_{22} & s_{24} \\ s_{42} & 44 \end{pmatrix} \begin{bmatrix} s_{2r} \\ s_{4r} \end{bmatrix} \tag{30}$$

$$F(s) = \frac{34.6360s^4 + 564.1179s^2}{s^4 + 14s^3 + 73.5s^2 + 171.5s + 150.0625} \tag{31}$$

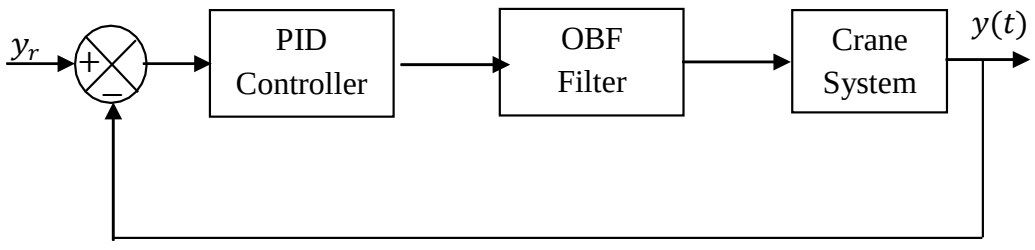

Fig. 6 - block diagram of PID-OBF controllers

3.3 Higher-Order Differential Feedback Controller

The design of a higher-order differential feedback controller was proposed in [33]. The application of this type of controller was achieved in chaos control, inverted pendulum control and other nonlinear systems. The differential equation of the nonlinear system with disturbance can be represented as a single input single output (SISO) affine system given in Eq. (32);

$$y^n = f(x) + b(x)u + d(t) \tag{32}$$

Where u and y are real numbers and are the control system input and output respectively. Also, $x = y^T$ represents the output differential vector, which is the same as the system state vector, y^i is the i^{th} differential of y and $f(.)$ is an unknown bounded affine function and $d(t)$ is bounded disturbance to the system.

The design of the controller is divided into three stages. The first stage involves the derivation of an error-based state-space model of the system using the observed states. The input and output of the reference signals of the system will be used to carry out the observations respectively hence resulting to the process second step, which is the design of an appropriate higher-order differentiator (HOD) for the particular problem that will extract the observed states formulated in the first step. The reference input signal, y is being processed by the HOD system at the input stage. This is done so as to obtain the required derivatives and extract the observed states. The output signal, y is being measured by the second HOD system after the injection of noise into the system. This is done to achieve a better estimation of the output and its required derivatives. Finally, a model-free pole placement procedure is applied with a filter to smoothen and complete the design of the higher-order differential feedback controller (HODFC).

• Step 1: Error Derivation with its Derivatives and the Observed States

The derivation of the error variable and its derivatives become possible based on the assumption that the output of the affine system in Eq. (32) is required to track an input trajectory $y_r(t)$ and that all derivatives of both $y_r(t)$ and y(t) are available as shown in Eq. (33);

$$e = y_r - x,\ \dot{e} = \dot{y}_r - \dot{x}, \ldots,\ e^n = y_r^n - \dot{x}_n \tag{33}$$

It is possible therefore to obtain an error-based state-space system that can be written as in Eq. (33) since the error and all its derivatives are available;

$$\begin{aligned} \dot{e}_1 &\equiv e_2 \\ \dot{e}_2 &\equiv e_3 \\ &\vdots \\ \dot{e}_n &\equiv y_r^n - y_n \end{aligned} \tag{34}$$

Hence, one can re-arrange the error vector as in Eq. (35) and its extended form can be written in Eq. (36);

$$e = y_r - x = \left[e, e_1, e, \ldots e_n\right]^T = \left[e, e^1, e^2, \ldots e^{n-1}\right]^T \tag{35}$$

$$\bar{e} = \bar{y}_r - \bar{x} = \left[e^T, e^n\right]^T \tag{36}$$

Considering the system in which the input y_r and the output y are known, the unknown can be estimated using Eq. (37). The next step shows how the observed states of the estimating vector x or y_r can be obtained using HOD.

$$\hat{\bar{x}} = \left[\hat{y}_r, \hat{y}_r^1, \hat{y}_r^2, \ldots, \hat{y}_r^n\right]^T \quad ; \quad \hat{\bar{y}}_r = \left[\hat{y}_r, \hat{y}_r^1, \hat{y}_r^2, \ldots, \hat{y}_r^n\right]^T \tag{37}$$

• Step 2: Design of Higher Order Differentiator (HOD)

For an m^{th} order system, the Higher Order Differentiator as well as the n^{th} order differential system of the HOD can be decided for which $n \geq m+1$. The HOD system can be obtained from two model-free parameters n and n_o, with $k_o \in [2,50]$ as in [34]. The parameters can be determined as in Eq. (38) and Eq. (39). Two copies of the HOD system were used in the controller structure as shown in Fig. 7. The block diagram of HODFC with the filters is shown in Fig. 7.

$$K = \frac{n^n}{(n-1)^{n-1}} \tag{38}$$

$$a_i = n_0^{i-1} K C_{n-1}^{i-1}, i = 1, 2, \ldots, n \tag{39}$$

To process some measurement *y(t)* using the HOD system, the *n*-system of integrators used for implementing the HOD is shown in Eq. (40);

$$\begin{cases} \dot{z}_i = z_{i+1} + a_i(\gamma - z_1) \\ z_k = a_k(\gamma - z_1) \qquad 1 \le i \le k-1 \\ \gamma = y(t) + \omega(t) \end{cases} \tag{40}$$

Where *Y(t)* measures the output y(t) with noise w(t) associated to it, with $z_1,\ldots,z_k$ being the states of the system. However, Eq. (41) can be used to determine the estimates of y(t) as;

$$\begin{cases} \hat{y} = z_1 \\ \hat{y} = z_{i+1} + a_i(\gamma - z_1) \qquad i = 1, 2, \ldots, n \end{cases} ; \quad \lim_{t \to 0} \hat{y}^i \equiv y^i \tag{41}$$

• Step 3: Pole placement procedure

Considering the final stage of the design of the higher-order differential feedback controller, K_e is used in place of Eq. (34) leading to Eq. (42);

$$y_r^n - y^n = Ke = k_1 e_1 + k_2 e_2 + \mathrm{K} + k_n e_n \tag{42}$$

For the polynomial $k_1+k_2S+k_3S^2+\ldots+k_nS^{n-1}+S^n$ to be Hurwitz polynomial, the elements of a vector K are chosen appropriately. Also, the structure of the pole placement can be represented by Eq. (36) as;

$$u = Ke + \hat{u} \tag{43}$$

With u as control force, the filtering signal from the control force can be expressed as in Eq. (44), where λ is a positive constant.

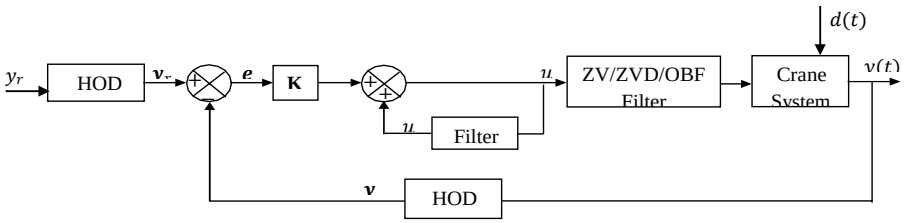

Fig. 7 – block representation of HODFC-ZV/ZVD/OBF

$$\dot{\hat{u}} = -\lambda \hat{u} + u \tag{44}$$

However, for the system under consideration, parameters of the higher-order differential feedback controller were selected for values of n = 3, a_0 = 8 and K = [-0.0035, 14.9048, 1], while 70/(S+70) was used for the filter function.

4. Results and Discussion

The input to the Crane system is a unit step which was simulated in MATLAB software to assess the performances of the hybrid controllers. A comparative analysis of PID-OBF, PID-ZV, PID-ZVD, HODFC-OBF, HODFC-ZV and HODFC-ZVD hybrid controllers for precise tracking control of payload was carried out. Firstly, the filters were designed to suppress the sway as follows:

• Output-based filter was designed using the system output and significant sway reduction was achieved as shown in Fig. 8 and Fig. 9.

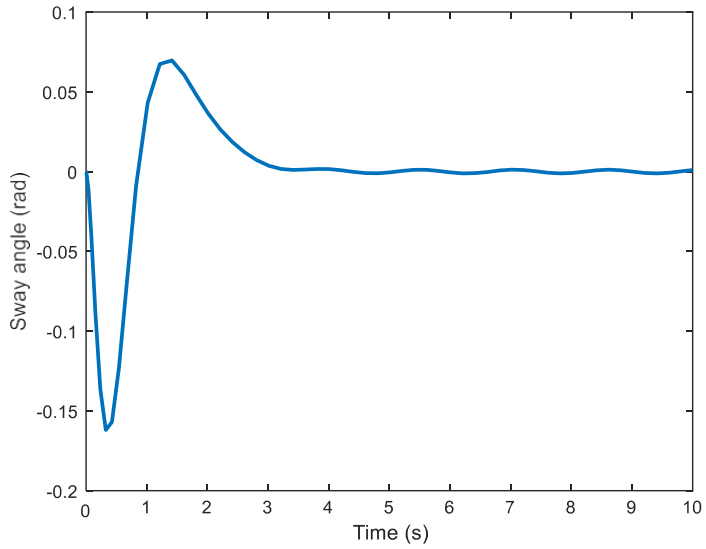

Fig. 8 - Sway angle response using OBF

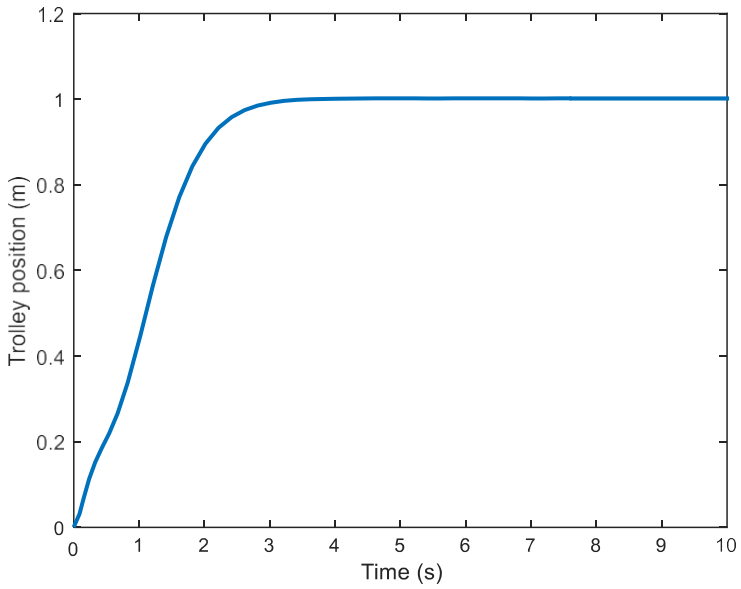

Fig. 9 - Trolley position travel using OBF

• Time delay filters were designed using the damping ratio and natural frequency of the system which were obtained using curve fitting toolbox in the MATLAB. In this type of filter, ZV and ZVD filters were considered and their response is shown in Fig. 10.

Secondly, higher-order differential feedback controller (which is non-model dependent) was incorporated with each filter for precise tracking control of the payload. Then, filters were also incorporated with the PID controller to validate the performances of the HODFC controller:

• The filters, ZV, ZVD and OBF were incorporated with HODFC controller for tracking control. And the filter was designed as 2/(s+2). Thus, a precise tracking was achieved with minimum sway, as can be observed in Fig. 11 and Fig. 12.

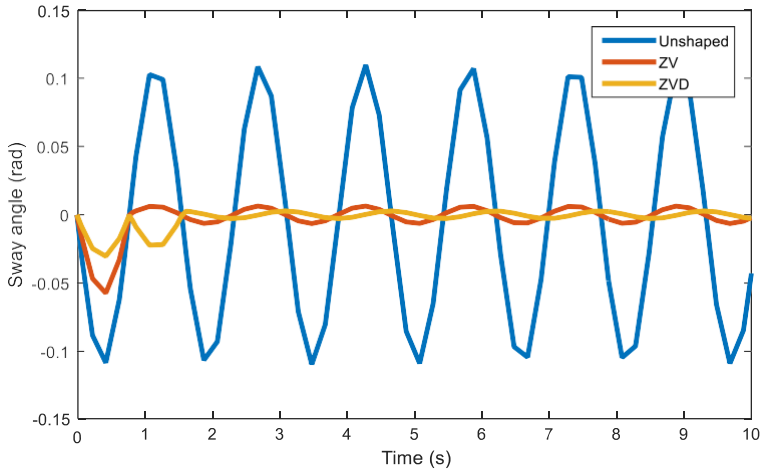

Fig. 10 - Sway angle response using time delay filters

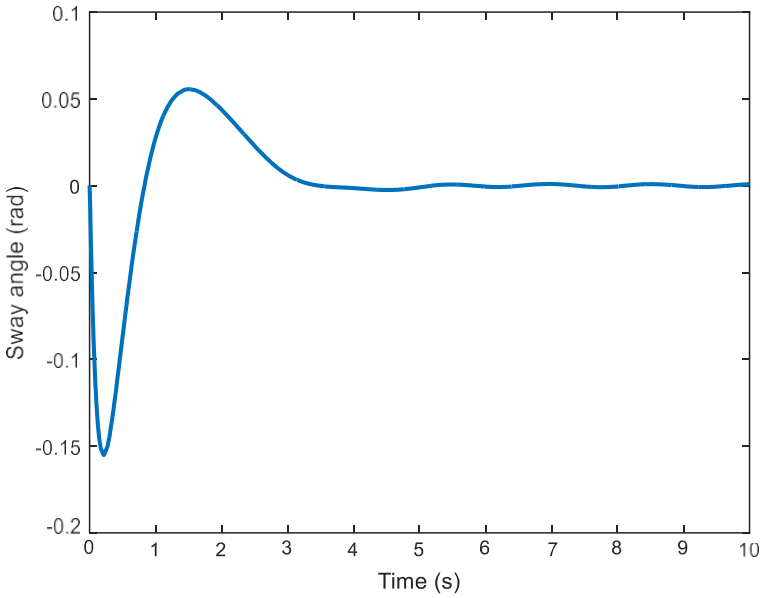

Fig. 11 - Sway angle using HODFC-OBF

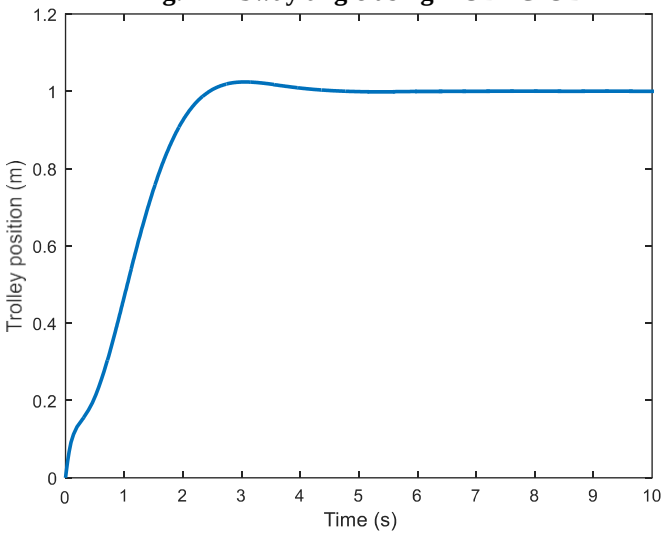

Fig. 12 - Trolley position travel using HODFC-OBIS

The HODFC was also incorporated with ZV and ZVD and the optimized gains were obtained as n = 3, a_o = 8, K= [-0.0035, 14.9048, 1] and the filters were designed as 70/(s+70); here again, a good tracking control with minimum sway was achieved as can be observed in Fig.13 to Fig. 16.

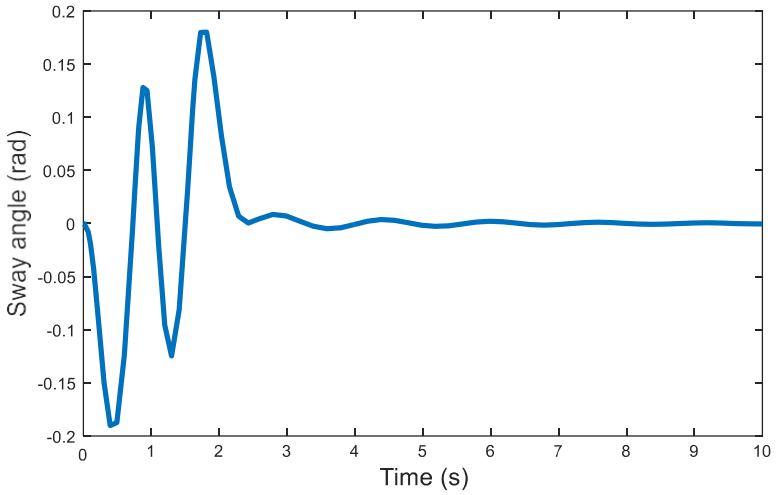

Fig. 13 - Sway angle using HODFC-ZV

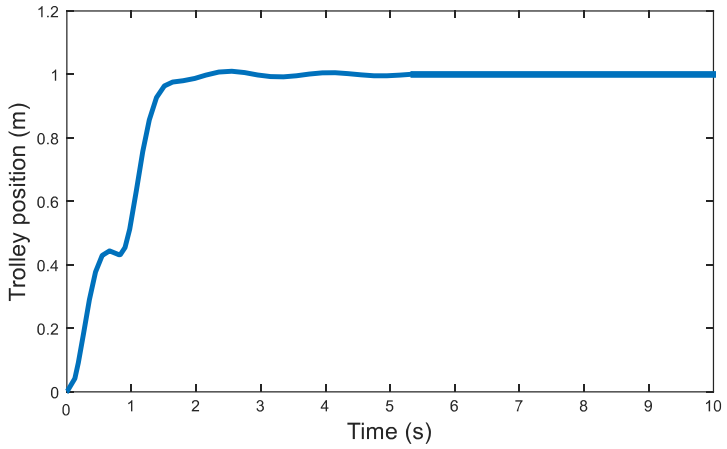

Fig. 14 - Trolley position travel using HODFC-ZV

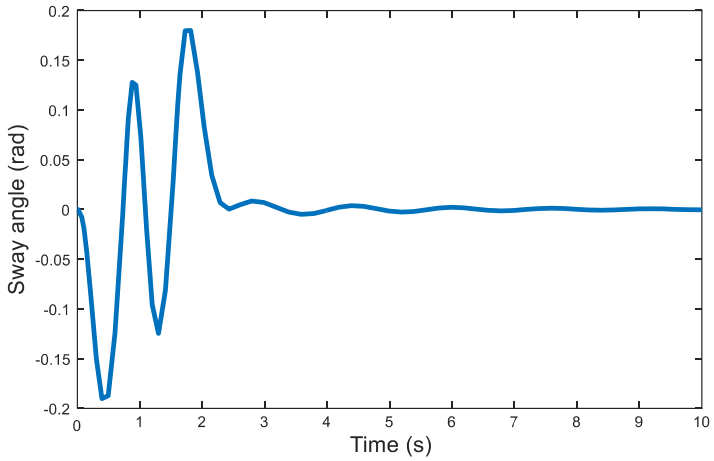

Fig. 15 - Sway angle using HODFC-ZVD

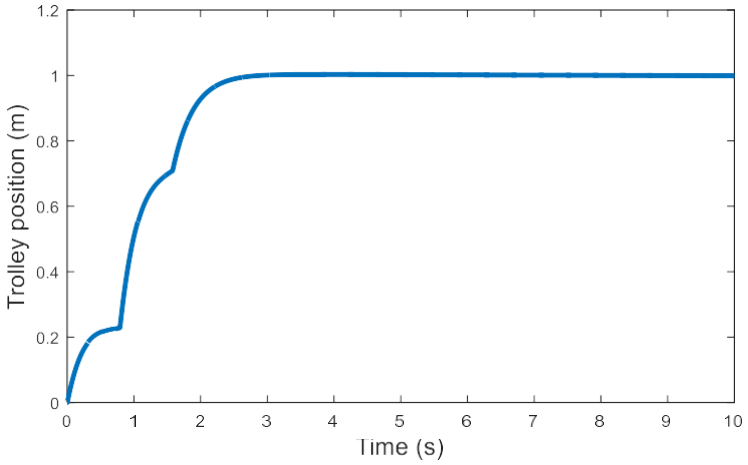

Fig. 16 - Trolley position travel using HODFC-ZVD

Moreover, hybrid PID control was proposed to validate the performances of the hybrid HODFC control schemes. Fig. 17 to Fig. 21 compared the tracking and sway reductions control performances of the controllers. Using mean absolute error and integral absolute error as the performance's indices, the performances of the hybrid controllers for sway reduction was assessed and compared as in Table 3.

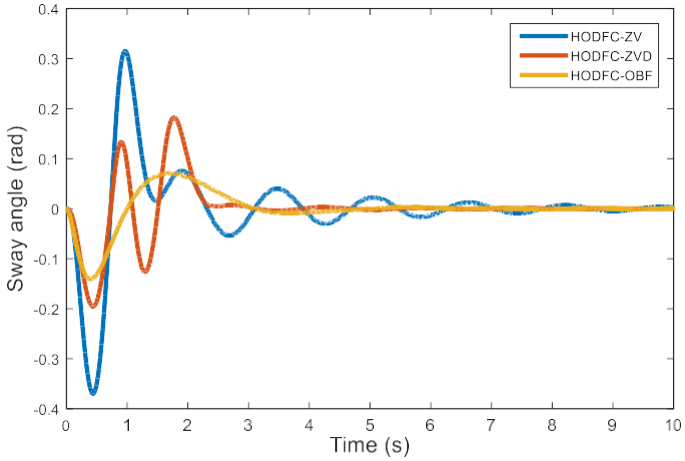

Fig. 17 - Sway angle comparison for HODFC-ZV/ZVD/OBF

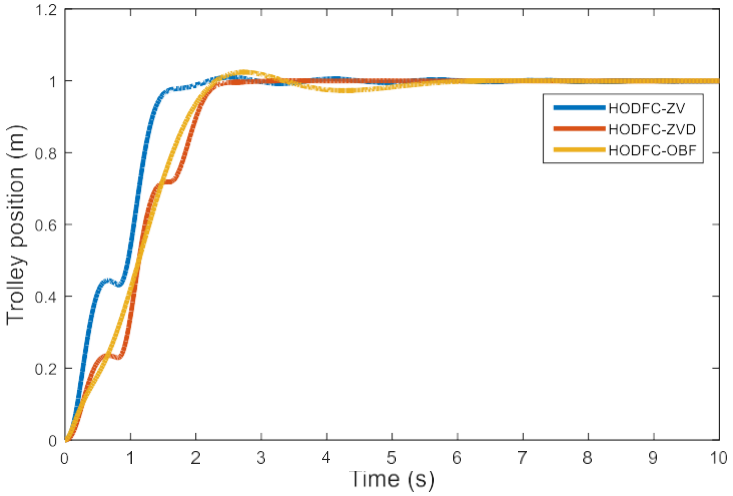

Fig. 18 - Trolley position travel for HODFC-ZV/ZVD/OBF

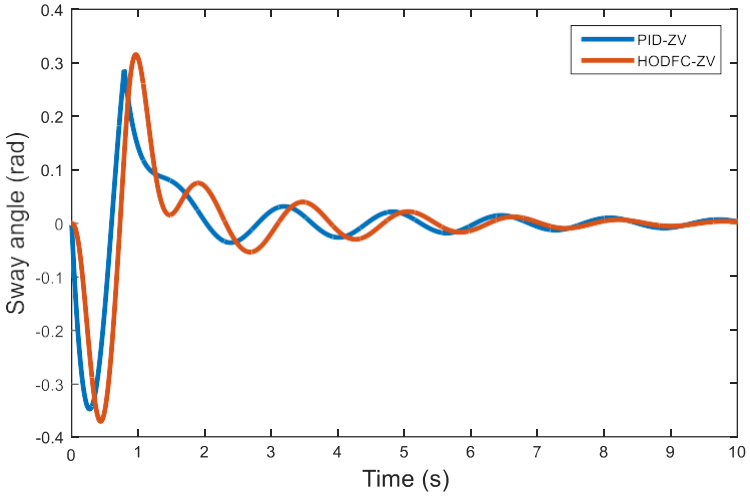

Fig. 19 - Sway angle comparison for PID/HODFC-ZV

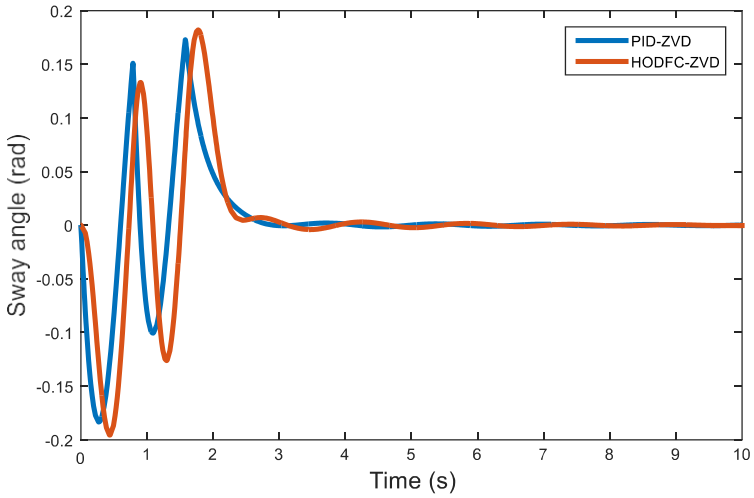

Fig. 20 - Sway angle comparison for PID/HODFC-ZVD

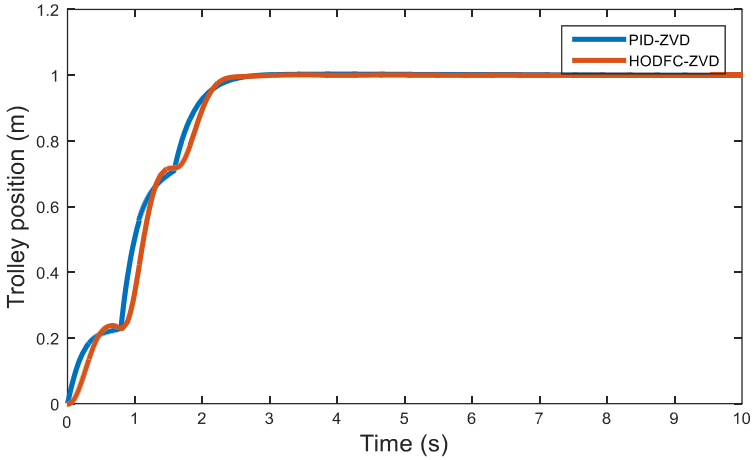

Fig. 21 - Trolley position travel comparison for PID/HODFC-ZVD

Table 3 - Time response and performance analyses

Controllers	Max. Overshoot (%)	Settling Time (s)	Rise Time(s)	ISE	IAE	Sway Reduction (MAE in %)
HODFC-ZV	1	1.365	1.195	$6.78x10^{-6}$	$6.02x10^{-6}$	77
HODFC-ZVD	0.1	2.145	1.728	$5.73x10^{-6}$	$6.43x10^{-6}$	79
HODFC-OBF	2.3	2.06	2.043	$4.59x10^{-6}$	$5.11x10^{-6}$	95
PID-ZV	0.6	1.435	1.268	$6.24x10^{-6}$	$6.91x10^{-6}$	76
PID-ZVD	0.2	2.12	1.726	$5.01x10^{-6}$	$5.01x10^{-6}$	88
PID-OBF	2.3	2.11	1.799	$4.33x10^{-6}$	$5.20x10^{-6}$	96

5. Conclusion

In this work, position tracking and sway suppression control of the crane system have been proposed using HODFC hybrid controller and the performances of the controller were validated with hybrid PID controller. The MAE, ISE and IAE were used as the performance indices and comparative studies using time response analysis were also presented. Simulation study and results analysis showed that a precise set-point tracking control and 96% sway suppression was achieved. In addition, HODFC hybrid control schemes are model-free controllers; hence they are robust to both internal and external disturbances. In the future, an experimental analysis would be conducted to verify these control schemes.

Acknowledgement

The authors wish to acknowledge the Universiti Technology, Malaysia (UTM) and Abubakar Tafawa Balewa University, Bauchi, for their tremendous support in carrying out this research.

References

[1] Singhose, W. (2009). Command shaping for flexible systems: A review of the first 50 years, International Journal of Precision Engineering and Manufacturing, 10, 153-168

[2] Hongjun, C., Bingtuan, G., & Xiaohua, Z. (2005). Dynamical modelling and nonlinear control of a 2D crane, in Proceedings of International Conference on Control and Automation, 2, 1085-1090.

[3] Jisup, Y., Nation, S., Singhose, W., & Vaughan, J. E. (2014). Control of Crane Payloads That Bounce During Hoisting, IEEE Transactions on Control Systems Technology, 22, 1233-1238.

[4] Alhassan, A. B., Muhammad, B. B., Danapalasingam, K. A., & Sam, Md. (2015). Optimal analysis and control of 2D nonlinear gantry crane system, 1st International Conference on Smart Sensors and Applications. Kuala Lumpur, Malaysia, p. 30–5.

[5] Garrido, S., Abderrahim, M., Giménez, A., Diez, R., & Balaguer, C. (2008). Anti-swinging input shaping control of an automatic construction crane, Automation Science and Engineering, IEEE Transactions, 5, 549-557.

[6] Tahir, N. M., Ibrahim, A. G. & Liman, H. (2017). Hybrid Control of Non-linear Crane System, Journal of Mechanical Engineering and Technology, 9, 71-86.

[7] Akbarimajd, A. (2015). Reinforcement Learning Adaptive PID Controller for an Under-Actuated Robot Arm. International Journal of Integrated Engineering 7 (2): 20–27.

[8] Annisa, J., Mat Darus, I. Z., Tokhi, M. O., & Abidin, A. S.Z. (2018). Controlling the Non-Parametric Modeling of Double Link Flexible Robotic Manipulator Using Hybrid PID Tuned by P-Type ILA. International Journal of Integrated Engineering 10 (7): 219–32.

[9] Sultan, N. M., Badrul Aisham, M. Z., Fatin, F. A., Yahya, M. S., Idris, A. L., & Hat, M. K. (2019). Modeling and Speed Control for Sensorless DC Motor BLDC Based on Real Time Experiment. International Journal of Integrated Engineering 11 (8): 55–64.

[10] Akbarimajd, A., & Amir, J.A.H. (2015). Multi-Agent Optimal Control of Ball Balancing on a Mobile Robot. International Journal of Integrated Engineering 7 (2): 14–19.

[11] Nafea, M., Colin, S., Suhail, K., Zaharuddin, M., & Mohamed, S. M. A. (2017). Optimal Two-Degree-of-Freedom Control for Precise Positioning of a Piezo-Actuated Stage. International Journal of Integrated Engineering 9 (4): 93–102.

[12] Nagarajan, D., Kavikumar, J., Lathamaheswari, M., & Broumi, S. (2019). Intelligent System Stability Using Type-2 Fuzzy Controller. International Journal of Integrated Engineering 11 (1): 270–82.

[13] Singer, N. C. and Seering, W. P. (1990). Preshaping command inputs to reduce system vibration. Journal of Dynamic Systems, Measurement, and Control, 12, 76-82

[14] Singhose, W. E., Seering, W. P. & Singer, N. C. (1990). Shaping inputs to reduce vibration: a vector diagram approach, IEEE Proceedings of International Conference on Robotics and Automation, 2, 922-927.

[15] Singhose, W., Singer, N. C. & Seering, W. P. (1994). Design and implementation of time-optimal negative input shapers, Proceedings of the 1994 International Mechanical Engineering Congress and Exposition, 151-157.

[16] Sorensen, K. L., Hekman, K. & Singhose, W. E. (2010). Finite-state input shaping, Control Systems Technology. IEEE Transactions, 18, 664-672.
[17] Singhose, W., Derezinski, S. & Singer, N. (1996). Extra-insensitive input shapers for controlling flexible spacecraft. Journal of Guidance, Control, and Dynamics, 19, 385-391.
[18] Crain, E. A., Singhose, W. E. & Seering, W. P. (1996). Derivation and properties of convolved and simultaneous two-mode input shapers, in IFAC World Congress, 441-446.
[19] Pao, L. & Singhose, W. (1996). Unity magnitude input shapers and their relation to time-optimal control, in IFAC World Congress, 385-390.
[20] Alhassan, A. B., Mohamed, Z., Abdullahi, A. M., Bature, A. A., Harun, A. & Tahir N. M. (2018). Input shaping comparison for sway control of rotary crane system, Journal Teknologi, 80, 61-69.
[21] Xiangguo, L., Zhiqian, M., Denglin, Z., & Baochun, X. (2017). Modeling and anti-sway control of ship-mounted crane. Advances in Mechanical Engineering. 9(9), 1-9.
[22] Sahinkaya, M. (2001). Input shaping for vibration-free positioning of flexible systems, Proceedings of the Institution of mechanical engineers, part I: Journal of Systems and Control Engineering, 215, 467-481.
[23] Xie, X., Huang, J., & Liang, Z. (2013). Using the continuous function to generate shaped command for vibration reduction, Proceedings of the Institution of Mechanical Engineers, Part I: Journal of Systems and Control Engineering, 227, 523-528.
[24] Singhose W. & Vaughan, J. (2011). Reducing vibration by digital filtering and input shaping, IEEE Transactions on Control Systems Technology, 19, 1410-1420.
[25] Biswas, S. K., (2004). Optimal control of gantry crane for minimum payload oscillations, Proceedings of Dynamic Systems and applications. Atlanta, USA, 12-19.
[26] Yoshida, Y. & Tabata, H. (2008). Visual feedback control of an overhead crane and its combination with time-optimal control. Proceedings of IEEE/ASME International Conference on Advanced Intelligent Mechatronics. Xian, China, 1114-1119.
[27] Mohd Tumari, M. Z., Shabudin, L., Zawawi, M. A., & Ahmad Shah, L. H. (2013). Active sway control of a gantry crane using hybrid input shaping and PID control schemes, IOP Conf. Series: Materials Science and Engineering, 50, 2-11.
[28] Ahmad, M. A., & Mohamed, Z. (2009). Hybrid Fuzzy Logic Control with Input Shaping for Input Tracking and Sway Suppression of a Gantry Crane System. American Journal of Engineering and Applied Sciences 2 (1), 241-251.
[29] Tahir, N. M., Abubakar, K. A., Jamil, M. M., Jahun, K. B., & Bala, F. S. (2018). Comparative Analysis of Input Shaping Techniques for Sway Control of Nonlinear Crane System. International Journal of Electrical Engineering and Applied Sciences, 1, 13-19.
[30] Tahir, N. M., Bature, A.A., Bature, U. I., Sambo, A.U., & Babawuro, A.Y. (2016). Vibration and Tracking Control of a Single-Link Flexible Manipulator Using LQR and Command Shaping. Journal of Multidisciplinary Engineering Science and Technology, 3, 45-67.
[31] Tahir, N. M. (2015). An Output-based Filter for Control of a Single-link Flexible Manipulator. Master, Universiti Teknologi Malaysia.
[32] Tahir, N. M., Hassan, S. M., Mohamed, Z., & Ibrahim, A. G. (2017). Output Based Input Shaping for Optimal Control of Single Link Flexible Manipulator. International Journal on Smart Sensing & Intelligent Systems, 10, 367-386.
[33] Nyabundi, S. A., Qi, G., Hamam, Y. & Munda, J. (2009). DC Motor Control via High Order Differential Feedback Control. *IEEE AFRICAN*. 1-5.
[34] Agee, J. T., Bingul, Z. & Kizir, S. (2015). Higher-order differential feedback control of a flexible-joint manipulator. Journal of Vibration and Control. 21 (10), 1976–1986.